

Photoexcitation of the one-dimensional extended Peierls-Hubbard model at quarter-filling

Yu-Peng Li(李昱澎), Yu-Chang Liu(刘羽畅), Yu-Zhuo Zhao(赵玉卓), Hantao Lu(陆汉涛), and Can Shao(邵灿)
Citation: Chin. Phys. B, 2026, 35 (**5**): 057104. DOI: 10.1088/1674-1056/ae27af
http://cpb.iphy.ac.cn; http://iopscience.iop.org/cpb

What follows is a list of articles you may be interested in

Electronic structure study of the intermetallic compound $GdRhIn_5$

Yulu He(贺宇璐), Bo Wang(王博), Xiangfei Yang(杨向飞), Dengpeng Yuan(袁登鹏), Wei Feng(冯卫), Yaobo Huang(黄耀波), and Qiuyun Chen(陈秋云)
Chin. Phys. B, 2026, 35 (**3**): 037101. DOI: 10.1088/1674-1056/ae3123

Numerical study of a quantum spin in an s-wave superconductor using the natural orbitals renormalization group method

Wen-Jing Zhang(张文静), Ru Zheng(郑汝), Rong-Qiang He(贺荣强), and Zhong-Yi Lu(卢仲毅)
Chin. Phys. B, 2026, 35 (**2**): 027104. DOI: 10.1088/1674-1056/adf4af

Charge self-consistent dynamical mean field theory calculations in combination with linear combination of numerical atomic orbitals framework based density functional theory

Xin Qu(瞿鑫), Peng Xu(许鹏), Zhiyong Liu(刘志勇), Jintao Wang(王金涛), Fei Wang(王飞), Wei Huang(黄威), Zhongxin Li(李忠星), Weichang Xu(徐卫昌), and Xinguo Ren(任新国)
Chin. Phys. B, 2024, 33 (**10**): 107106. DOI: 10.1088/1674-1056/ad6558

Heavy fermions in high magnetic fields

M Smidman, B Shen(沈斌), C Y Guo(郭春煜), L Jiao(焦琳), X Lu(路欣), H Q Yuan(袁辉球)
Chin. Phys. B, 2019, 28 (**1**): 017106. DOI: 10.1088/1674-1056/28/1/017106

Electronic structure and magnetic properties of rare-earth perovskite gallates from first principles

A Dahani, H Alamri, B Merabet, A Zaoui, S Kacimi, A Boukortt, M Bejar
Chin. Phys. B, 2017, 26 (**1**): 017101. DOI: 10.1088/1674-1056/26/1/017101

SPECIAL TOPIC — Exciton Physics: Fundamentals, materials and devices

Photoexcitation of the one-dimensional extended Peierls–Hubbard model at quarter-filling

Yu-Peng Li(李昱澎)[1,†], Yu-Chang Liu(刘羽畅)[1,†], Yu-Zhuo Zhao(赵玉卓)[1,†], Hantao Lu(陆汉涛)[2,3], and Can Shao(邵灿)[1,‡]

[1] *Department of Applied Physics & MIIT Key Laboratory of Semiconductor Microstructure and Quantum Sensing, Nanjing University of Science and Technology, Nanjing* 210094, *China*

[2] *School of Physical Science and Technology, Lanzhou University, Lanzhou* 730000, *China*

[3] *Lanzhou Center for Theoretical Physics, Key Laboratory of Theoretical Physics of Gansu Province, Key Laboratory of Quantum Theory and Applications of MoE, Gansu Provincial Research Center for Basic Disciplines of Quantum Physics, Lanzhou University, Lanzhou* 730000, *China*

(Received 7 September 2025; revised manuscript received 21 November 2025; accepted manuscript online 4 December 2025)

Utilizing the time-dependent Lanczos method, we investigate the photoexcitation dynamics of the one-dimensional (1D) extended Peierls–Hubbard model at quarter filling. In equilibrium, it is well established that introducing the nearest-neighbour interaction V into the 1D Peierls–Hubbard model can lead to the formation of Mott–Hubbard excitons, which exhibit a characteristic frequency in the optical conductivity that is lower than the Mott gap. Ultrafast photoexcitation of this model gives rise to a transient metallic state for $V < 2$, characterized by several features, including a zero-frequency Drude peak in the post-pump optical conductivity, an increase in the density of charge carriers, and enhanced electron hopping between dimers. In contrast, when $V \geq 2$, this metallic state is no longer observed, as photoinduced carriers bind to form excitons, thereby inhibiting metallic behavior. These results highlight a parallel between the optical excitation of the 1D extended Peierls–Hubbard model at quarter filling and that of the 1D extended Hubbard model at half filling, suggesting a universal mechanism governing their photoinduced responses.

Keywords: strongly correlated electron systems, extended Peierls–Hubbard model, ultrafast dynamics

PACS: 71.27.+a, 71.10.Fd, 78.47.J–

DOI: 10.1088/1674-1056/ae27af **CSTR:** 32038.14.CPB.ae27af

1. Introduction

Ultrafast optical techniques have opened a route to track and manipulate the dynamics of strongly correlated electrons on femtosecond timescales.[1,2] Such approaches have revealed a variety of nonequilibrium phenomena, ranging from light-induced metallicity in Mott insulators,[3–5] carrier redistribution in charge-density-wave materials,[6] to superconducting-like responses triggered by strong optical fields.[7–10] Recent ultrafast spectroscopy studies have also explored strongly correlated materials under high pressure.[11,12] These observations underscore the importance of understanding how photocarriers are generated, interact, and reorganize the underlying electronic background, thereby motivating extensive theoretical work based on Hubbard-type models to unravel the mechanisms governing these transient states.[13–29]

Organic charge-transfer salts constitute a class of materials whose low-energy electronic behavior is often effectively one-dimensional (1D) and highly susceptible to lattice modulations. In compounds such as $(EDO\text{-}TTF)_2PF_6$, ultrafast spectroscopy has revealed rapid switching between competing charge-ordered configurations,[30,31] thereby motivating the use of quarter-filled Peierls–Holstein variants of the Hubbard model to capture their underlying physics.[32–34] Even in the absence of Holstein coupling, the Peierls–Hubbard framework successfully describes the dimerized Mott-insulating ground state characteristic of several related materials.[35–43] A recent study further reported a photoinduced metallic phase in this model, where photoexcitation generates empty and doubly occupied dimers,[44] which serve as analogs of holons and doublons in standard Hubbard systems. Equilibrium studies on the extended Peierls–Hubbard model further reveal that the nearest-neighbor interaction V substantially reshapes the excitation spectrum by stabilizing Mott–Hubbard excitons and inducing pronounced shifts in the optical-absorption peak.[42] These features parallel those in the extended Hubbard model at half-filling, where equilibrium calculations identify a crossover between unbound holon–antiholon excitations and bound excitons as V increases.[45]

Despite the detailed equilibrium understanding of these models, comparatively little is known about how excitonic effects and dimerization influence the real-time evolution after photoexcitation. In this work, we examine the nonequilibrium dynamics of the 1D extended Peierls–Hubbard model at

[†] These authors contributed equally to this work.

[‡] Corresponding author. E-mail: shaocan@njust.edu.cn

© 2026 Chinese Physical Society and IOP Publishing Ltd. All rights, including for text and data mining, AI training, and similar technologies, are reserved.

quarter filling, focusing on the evolution of energies, photoinduced carriers, and optical conductivity following an ultrafast pump. Our analysis employs a nonequilibrium linear-response approach that captures the zero-frequency component of the optical conductivity under periodic boundary conditions. We show that for moderate nearest-neighbor interaction ($V = 1$), the photoinduced dynamics resemble those of the Peierls–Hubbard model without intersite repulsion, yielding clear signatures of transient metallic behavior. By contrast, for $V \geq 2$, the system fails to develop a metallic response, consistent with the persistent binding of photoinduced empty and doubly occupied dimers into excitonic pairs. These results demonstrate that the nonequilibrium response of the quarter-filled extended Peierls–Hubbard model exhibits a dynamical analog of the exciton crossover known from the half-filled extended Hubbard model, thereby establishing a direct link between equilibrium excitation structure and ultrafast photoinduced behavior.

The paper is organized as follows: in Section 2 we discuss the Hamiltonian model and the time-dependent optical conductivity relevant to the photoinduced dynamics; in Section 3 we present the results for the time-dependent behavior of the optical conductivity and other properties; and finally in Section 4 we close with the conclusions.

2. Model, method, and measurements

The 1D extended Peierls–Hubbard model takes the form $H = H_{\rm k} + H_U + H_V$, where the kinetic Hamiltonian reads

$$H_{\rm k} = -\sum_{i,\sigma}\left\{\left(t_{\rm h}\left[1+\delta(-1)^i\right]c^{\dagger}_{i,\sigma}c_{i+1,\sigma} + {\rm H.c.}\right\}, \tag{1}$$

and the interaction terms are

$$H_U = U\sum_i n_{i,\uparrow}n_{i,\downarrow}, \quad H_V = V\sum_i n_i n_{i+1}. \tag{2}$$

Here $c^{\dagger}_{i,\sigma}$, $c_{i,\sigma}$, and $n_{i,\sigma}$ are the creation, annihilation, and number operators of an electron at site i with spin σ, respectively. The operator $n_i = n_{i,\uparrow} + n_{i,\downarrow}$ denotes the total number of electrons at site i. The quantity $t_{\rm h}[1+\delta(-1)^i]$ represents the staggered hopping amplitude, and Eq. (1) corresponds to the Peierls term that describes a dimerized chain. U and V represent the strengths of the on-site and nearest-neighbor Coulomb interactions, respectively.

In the Weyl (temporal) gauge, the effect of the external electric field is incorporated via the Peierls substitution

$$\begin{aligned}&\left\{t_{\rm h}[1+\delta(-1)^i]c^{\dagger}_{i,\sigma}c_{i+1,\sigma} + {\rm H.c.}\right\}\\ \longrightarrow\ &{\rm e}^{{\rm i}A(t)}\left\{t_{\rm h}[1+\delta(-1)^i]c^{\dagger}_{i,\sigma}c_{i+1,\sigma} + {\rm H.c.}\right\},\end{aligned} \tag{3}$$

where the vector potential is given by

$$A(t) = A_0\cos\left[\omega_0(t-t_0)\right]{\rm e}^{\frac{-(t-t_0)^2}{2t_{\rm d}^2}}. \tag{4}$$

Here, t_0 denotes the pulse center, while $t_{\rm d}$ and ω_0 determine the temporal width and central frequency of the Gaussian envelope, respectively. The time-dependent wave function is computed using the time-evolving Lanczos method,[46] based on the following central formula:

$$|\psi(t+\delta t)\rangle \simeq \sum_{l=1}^{M}{\rm e}^{-{\rm i}\varepsilon_{\rm l}\delta t}|\phi_{\rm l}\rangle\langle\phi_{\rm l}|\psi(t). \tag{5}$$

Here, $\varepsilon_{\rm l}$ and $|\phi_{\rm l}\rangle$ denote the eigenvalues and eigenvectors, respectively, in the Krylov subspace constructed during the Lanczos procedure. For the numerical simulations, we adopt a time step of $\delta t = 0.02$ and take $M = 30$ to ensure the accuracy and reliability of the results.

To compute the time-dependent optical conductivity, we employ an approach formulated within the framework of nonequilibrium linear-response (NLR) theory,[47] whose validity has been discussed in detail in Refs. [19,44]. The key expressions used in this work are summarized in Appendix A. While the NLR approach provides optical conductivity both in and out of equilibrium, it is instructive to compare it with the standard Kubo formula, which applies only in equilibrium. We thus compute the equilibrium optical conductivity via the Kubo formula as a reference for the NLR results. The Kubo formula is written as

$$\begin{aligned}{\rm Re}\,\sigma(\omega) = &\frac{\pi}{L}\sum_{m\neq 0}\frac{1}{E_m - E_0}|\langle\Psi_m|j|\Psi_0\rangle|^2\\ &\times\delta[\omega-(E_m-E_0)].\end{aligned} \tag{6}$$

The key distinction between the two methods lies in the fact that the Kubo formula circumvents the need for time evolution; however, it fails to capture the zero-frequency (Drude) weight since $m \neq 0$ in Eq. (6).

Additionally, we define the time-dependent order parameter of the spin-density-wave (SDW) order as

$$\mathcal{O}_{\rm SDW}(t) = \langle\psi(t)|O_{\rm SDW}|\psi(t)\rangle, \tag{7}$$

where the operator $O_{\rm SDW}$ reads

$$O_{\rm SDW} = \frac{1}{L^2}\sum_{i=0}^{L-1}\sum_{j=0}^{L-1}(-1)^{j-i}(n_{i,\uparrow}-n_{i,\downarrow})(n_{j,\uparrow}-n_{j,\downarrow}).$$

Note that the indices i and j refer to the unit cells, i.e., the dimers, rather than individual sites.

In what follows, we set $U = 9$ and $\delta = 0.5$, and consider a periodic chain of $L = 12$ sites, corresponding to $L/2 = 6$ unit cells (dimers). Energy and time are measured in units of $t_{\rm h}$ and ${t_{\rm h}}^{-1}$, respectively. Our analysis focuses on the real part of the optical conductivity, i.e., Re $\sigma(\omega, t)$.

3. Results

We first present the equilibrium optical conductivity of the extended Peierls–Hubbard model at quarter filling, Re $\sigma(\omega)$, as shown in Fig. 1 for various V. Results obtained from the NLR method (blue lines) are compared with those from the Kubo formula (black lines). The NLR method reveals that the zero-frequency optical conductivity (the Drude peak) does not completely vanish for $V = 0$ in Fig. 1(a), even though the system is in an insulating state. As reported in Ref. [48], the Peierls–Hubbard model at quarter filling with $V = 0$ exhibits a small single-particle gap even for sufficiently large U. Therefore, the non-vanishing Drude peak observed at $V = 0$ arises from finite-size effects[19,44] in systems with a small gap. On the other hand, the Drude peak gradually decreases and eventually vanishes as V increases, as shown in Figs. 1(b)–1(f) for $V = 1$, $V = 2$, $V = 3$, $V = 4$, and $V = 5$, respectively. This behavior reflects the fact that the nearest-neighbour interaction V can significantly enhance the single-particle gap, as illustrated in Fig. 4 of Ref. [48].

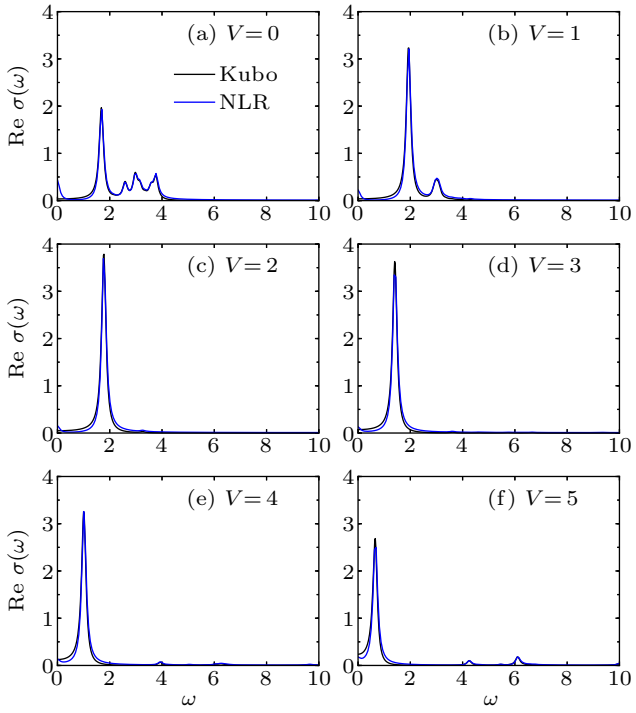


Fig. 1. Equilibrium optical conductivity Re $\sigma(\omega)$ of the quarter-filled extended Peierls–Hubbard model ($L = 12$, $U = 9.0$, $\delta = 0.5$) for (a) $V = 0.0$, (b) $V = 1.0$, (c) $V = 2.0$, (d) $V = 3.0$, (e) $V = 4.0$, and (f) $V = 5.0$. Black lines denote results obtained from the Kubo formula, while blue lines represent those from the nonequilibrium linear-response (NLR) approach.

In addition to the Drude peak, the main absorption peak shifts slightly toward higher frequencies as V increases from 0 to 1. Note that the position of the main absorption peak is commonly defined as the optical gap. However, as V further increases from 1 to 5, the optical gap decreases, in contrast to the behavior of the single-particle gap reported in Ref. [48]. This phenomenon has also been observed and discussed in Ref. [42] using the dynamical density matrix renormalization-group (DDMRG) method. Their study found that, in the limit of an infinite chain, the optical gap extrapolates to a smaller value than the Mott gap due to the formation of Mott–Hubbard excitons, which become more tightly bound as V increases. Consequently, the optical gap gradually shifts from a value above the Mott gap to the excitonic peak (δ-peak) below the Mott gap.

Meanwhile, the spectral structures located at $\omega \in [2,4]$ in Fig. 1(a) — which, as discussed in Ref. [44], can be associated with energy differences between various single-particle bands (see also Ref. [48]) — gradually lose spectral weight as V increases from 0 to 3. We attribute this behavior to the increasing dominance of excitonic excitations, which suppress the contributions from single-particle excitations. As V increases to 5 and 6, these spectral features shift to higher frequencies ($\omega \gtrsim 4$) due to the further enlargement of the single-particle gap (see Ref. [48]) and begin to regain spectral weight, while the δ-like exciton peak correspondingly loses weight. This behavior arises because a larger single-particle gap makes it increasingly difficult to generate empty and doubly occupied dimers, thereby weakening their binding and suppressing exciton formation. Note that the results reported in Refs. [44,48], which primarily focus on $U = 10$, are qualitatively similar to those obtained with $U = 9$. In this work, we choose $U = 9$ to avoid redundancy.

To explore the formation of excitons, we apply a pumping pulse to excite the system and analyze its nonequilibrium dynamics. We define $\Delta t = t - t_0$ as the time interval between the probing time and t_0, where t_0 denotes the peak time of the pumping pulse. The parameters of the pumping pulse are specified as follows: the amplitude is set to $A_0 = 0.2$, the pulse width is determined by $t_d = 2.0$, and the frequency ω_0 is chosen to align with the optical gap, i.e., the frequency of the primary absorption peak in the equilibrium optical conductivity.

Setting the nearest-neighbor interaction $V = 1$ ($\delta = 0.5$ and $U = 9$), Fig. 2(a) displays the results of Re $\sigma(\omega, \Delta t)$ for $\Delta t = -\infty$, 10, 20 and 30, represented by different colors. Here, $\Delta t = -\infty$ corresponds to the system's equilibrium optical conductivity, i.e., before the arrival of the pump pulse. After photoirradiation, a positive peak emerges at very low frequencies, while a negative peak appears at zero frequency. For clarity, we refer to the former as the in-gap peak, as it lies below the original optical gap, and the latter as the Drude peak. Interestingly, in Fig. 2(a) of Ref. [44] ($\delta = 0.5$, $U = 10$ and $V = 0$), the Drude peak is positive and the in-gap peak is negative. We have verified that the case of $U = 9$ and $V = 0$ yields results similar to those of $U = 10$ and $V = 0$, which are not shown here to avoid redundancy. The underlying mechanism has been thoroughly analyzed in Refs. [44,49]. It stems from an excitation transition from an odd-parity excited state (whose energy

corresponds to the primary absorption peak) to an even-parity excited state following the pump. If the energy of the even-parity excited state is higher (lower) than that of the odd-parity excited state, the in-gap peak manifests as a positive absorption peak (negative emission peak). As a result, we speculate that the nearest-neighbor interaction V increases the energy of the even-parity excited state, making it higher than that of the odd-parity excited state. This interpretation is further supported by the results for $V = 2$, as shown in Fig. 3(a) below. Regardless of whether the in-gap peak is positive or negative, it is a consequence of finite-size effects and can be interpreted as an indicator of a metallic state.[44,50] On the other hand, the prominent absorption peak at $\omega = 1.94$ in the optical conductivity not only diminishes in intensity but also transitions into a negative weight after photoirradiation. This phenomenon occurs because the excited state associated with this peak significantly contributes to the time-evolving wave function. As a result, the optical conductivity at this frequency weakens in intensity or even inverts into a negative emission peak.

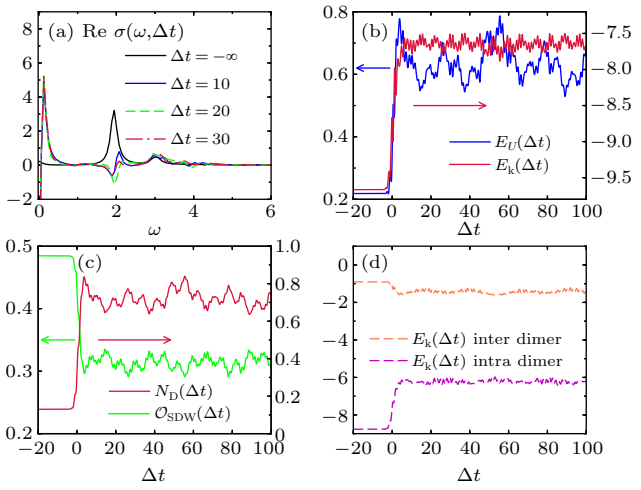


Fig. 2. (a) Optical conductivity $\mathrm{Re}\sigma(\omega,\Delta t)$ at $\Delta t = -\infty$, 10, 20, and 30; (b) kinetic energy $E_k(\Delta t)$ and interaction energy $E_U(\Delta t)$; (c) number of doubly occupied dimers N_D; and (d) inter- and intra-dimer kinetic energies as functions of time. Model parameters: $L = 12$, $\delta = 0.5$, $U = 9.0$, and $V = 1.0$. Pump pulse parameters: $A_0 = 0.2$, $t_d = 2.0$, and $\omega_0 = 1.94$.

Other features of the photoexcitation dynamics in the extended Peierls–Hubbard model closely resemble those of the Peierls–Hubbard model described in Ref. [44]. For instance, the interaction energy E_U increases from 0.22 to an average value of approximately 0.65 after the application of the pump pulse, as illustrated in Fig. 2(b). From Eq. (2), which gives $E_U = Un_d$, where n_d represents the number of doubly occupied sites and $U = 9$, we find that n_d increases from 0.024 to approximately 0.072 in a 12-site chain. We consider this increase too small to generate a metallic state.

If we define N_D as the number of doubly occupied dimers — specifically, dimers containing one spin-↑ electron and one spin-↓ electron — we find that the increase in N_D is about 0.2 for the 6-dimer chain, as shown in Fig. 2(c). As discussed in Ref. [44], empty and doubly occupied dimers play the role of photoinduced charge carriers. On the other hand, the increase in kinetic energy E_k is significantly larger than that of the interaction energy E_U, as shown in Fig. 2(b). The kinetic energy comprises two components: the intra-dimer and inter-dimer contributions. These are displayed in Fig. 2(d), where we observe that the intra-dimer kinetic energy increases, whereas the inter-dimer kinetic energy decreases. This behavior suggests that the pump pulse enables electrons to overcome the barriers between dimers, thereby increasing the number of empty and doubly occupied dimers.[44]

Additionally, we observe the collapse of the original SDW state (an antiferromagnetic Mott insulator in units of dimers), as shown in Fig. 2(c).

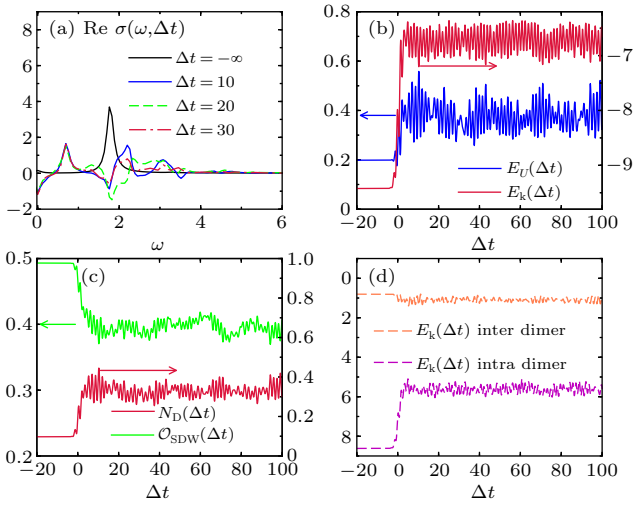


Fig. 3. Same properties as those shown in Fig. 2. Model parameters: $L = 12$, $\delta = 0.5$, $U = 9.0$, and $V = 2.0$. Pump pulse parameters: $A_0 = 0.2$, $t_d = 2.0$, and $\omega_0 = 1.78$.

We now examine the nonequilibrium dynamics for $V = 2$, as illustrated in Fig. 3. Similar to the case of $V = 1$, a negative Drude peak and a positive in-gap peak appear after the pump. However, the frequency of the in-gap peak is higher than that for $V = 1$, as shown in Fig. 3(a) and compared with Fig. 2(a). This shift occurs because the increased nearest-neighbor interaction V further raises the energy of the even-parity excited state. Additionally, the intensity of the in-gap peak is lower than that for $V = 1$, suggesting a suppression of the photoinduced metallic state.

Meanwhile, both the number of doubly occupied sites n_d (as inferred from the interaction energy E_U in Fig. 3(b)) and the number of doubly occupied dimers N_D (see Fig. 3(c)) show only slight increases. Furthermore, the collapse of the SDW state is less pronounced compared to the case of $V = 1$. The kinetic energy E_k increases more significantly than in the case of $V = 1$ (see Figs. 2(b) and 3(b)), primarily due to the increase in intra-dimer kinetic energy. In contrast, the change in inter-dimer kinetic energy is minimal compared to that for $V = 1$ (see Figs. 2(b) and 3(b)). Note that a decrease in inter-dimer

kinetic energy typically indicates enhanced electron mobility between dimers.

Taken together, these features — reduced in-gap peak intensity, limited increases in $n_{\rm d}$ and $N_{\rm D}$, a less pronounced collapse of the SDW state, and minimal changes in inter-dimer kinetic energy — collectively indicate a suppression of the photoinduced metallic state for $V = 2$. Based on optical excitations in the 1D extended Hubbard model (without the Peierls term),[45] where unbound holon–antiholon pairs dominate for $V < 2$ and excitons (bound holon–antiholon pairs) form for $V > 2$, we attribute the suppression of the photoinduced metallic state to the emergence of exciton formation at $V = 2$, where the binding of empty and doubly occupied dimers reduces charge carrier mobility.

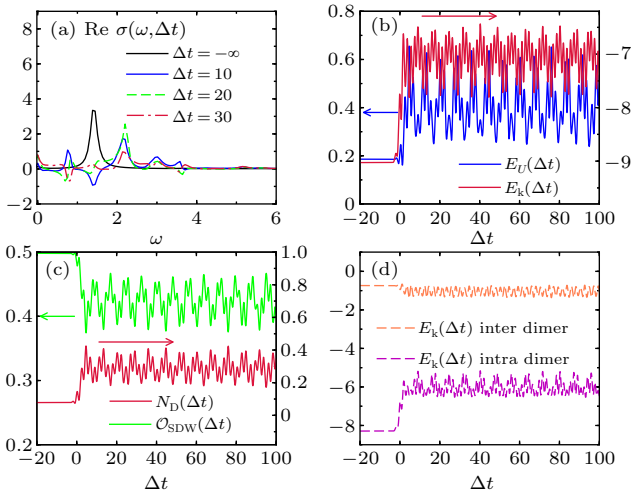


Fig. 4. Same properties as those shown in Fig. 2. Model parameters: $L = 12$, $\delta = 0.5$, $U = 9.0$, and $V = 3.0$. Pump pulse parameters: $A_0 = 0.2$, $t_{\rm d} = 2.0$, and $\omega_0 = 1.4$.

For $V = 3$, where excitonic binding is expected to be particularly robust, our time-resolved optical conductivity measurements ($\mathrm{Re}\,\sigma(\omega,\Delta t)$) reveal transient spectral features at delay times $\Delta t = 10$, 20, and 30, as shown in Fig. 4(a). We observe that the features below the optical gap ($\omega \approx 0.8$) exhibit significant temporal fluctuations, oscillating between absorption (positive) and emission (negative) character. This oscillatory behavior contrasts with the stable in-gap signatures observed at $V = 2$ and $V = 1$, and precludes their interpretation as signatures of a metallic phase. Other quantities of the system — including the kinetic energy, interaction energy, number of doubly occupied dimers, the order parameter of the SDW state, and inter-/intra-dimer kinetic energies (Figs. 4(b)–4(d)) — maintain similar average values to the $V = 2$ case (Figs. 3(b)–3(d)). However, for $V = 3$, these quantities exhibit regular oscillations after the pump. We attribute these dynamical features to a quantum superposition between bound excitonic states (comprising empty and doubly occupied dimers) and dissociated configurations (consisting of singly occupied spin-↑ and spin-↓ sites). This coherent mixing enables periodic restoration of the original antiferromagnetic order through quantum tunneling between these competing states. This interpretation is strongly supported by the antiphase oscillations between $\mathcal{O}_{\rm SDW}(\Delta t)$ and $N_{\rm D}(\Delta t)$ in Fig. 4(c), as well as the temporal fluctuations of the in-gap structures in the optical conductivity in Fig. 4(a). This dynamical picture naturally explains the suppression of metallic behavior while accounting for all observed oscillatory phenomena in the strong-coupling regime ($V = 3 > 2$). The quantum coherence between these distinct electronic configurations represents a novel manifestation of the competition between charge and spin degrees of freedom in correlated electron systems.

4. Conclusion

To summarize, we investigate the photoexcitation dynamics of the one-dimensional (1D) extended Peierls–Hubbard model at quarter filling using the time-dependent Lanczos method. In equilibrium, the introduction of nearest-neighbor interaction V leads to the formation of Mott–Hubbard excitons, which are characterized by an optical conductivity peak below the Mott gap. Under ultrafast photoirradiation, we observe a photoinduced metallic state for $V < 2$, evidenced by the Drude and in-gap peaks, an increase in charge carrier density (empty and doubly occupied dimers), and enhanced inter-dimer electron mobility. However, for $V \geq 2$, this metallic state is suppressed as photoinduced carriers bind to form excitons, thereby inhibiting metallic behavior. These results draw a parallel between the photoexcitation dynamics of the 1D extended Peierls–Hubbard model at quarter filling and the 1D extended Hubbard model at half filling. This work highlights the critical role of exciton formation in modulating nonequilibrium dynamics and provides insights into the interplay between interactions and photoexcitation in low-dimensional correlated systems.

Appendix A: Key formulas of the nonequilibrium linear-response theory

In the nonequilibrium linear-response theory, the two-time response function $\sigma(t',t)$ with the restriction $t' \geq t$ can be obtained from

$$\sigma(t',t) = \frac{1}{L}\left[\int_t^{t'} \chi(t',t'')\,\mathrm{d}t'' + \langle\psi(t')|\tau|\psi(t')\rangle\right], \quad \text{(A1)}$$

where

$$\tau = \sum_{i,\sigma}\left\{t_{\rm h}\,\mathrm{e}^{\mathrm{i}A(t)}\left[1+\delta(-1)^i\right]c^\dagger_{i,\sigma}c_{i+1,\sigma} + \text{H.c.}\right\}, \quad \text{(A2)}$$

$$\chi(t',t'') = -\mathrm{i}\theta(t'-t'')\langle\psi(t)|[j^I(t'), j^I(t'')]|\psi(t)\rangle. \quad \text{(A3)}$$

In the interaction representation, the current operator is given by $j^I(t') = U^\dagger(t',t)\, j\, U(t',t)$, where $U(t',t)$ is the time-evolution operator, and

$$j = -\mathrm{i}\sum_{i,\sigma}\left\{t_\mathrm{h}\,\mathrm{e}^{\mathrm{i}A(t)}\left[1+\delta(-1)^i\right]c^\dagger_{i,\sigma}c_{i+1,\sigma} - \mathrm{H.c.}\right\}. \quad \text{(A4)}$$

Finally, the time-dependent optical conductivity is obtained as

$$\sigma(\omega,t) = \int_0^{+\infty}\sigma(t+s,t)\,\mathrm{e}^{\mathrm{i}(\omega+i\eta)s}\,\mathrm{d}s, \quad \text{(A5)}$$

where the integration cutoff for s is taken to be one hundred time units and the broadening factor is $\eta = 0.1$. Further details of these formulas, derived within the framework of nonequilibrium linear-response theory, can be found in Refs. [19,44,47].

Acknowledgments

We thank H.-Q. Lin, T. Tohyama and L. Du for helpful discussions. C. S. and H. L. acknowledge supports from the National Natural Science Foundation of China (Grant No. 12247101), the Fundamental Research Funds for the Central Universities (Grant No. lzujbky-2025-jdzx07), the Natural Science Foundation of Gansu Province (Grant No. 25JRRA799), and the '111 Center' (Grant No. B20063). H. L. acknowledges support from the National Natural Science Foundation of China (Grants No. 12174168).

References

[1] Murakami Y, Golež D, Eckstein M and Werner P 2025 *Rev. Mod. Phys.* **97** 035001
[2] Hu S Q and Meng S 2023 *Chin. Phys. Lett.* **40** 117801
[3] Iwai S, Ono M, Maeda A, Matsuzaki H, Kishida H, Okamoto H and Tokura Y 2003 *Phys. Rev. Lett.* **91** 057401
[4] Okamoto H, Matsuzaki H, Wakabayashi T, Takahashi Y and Hasegawa T 2007 *Phys. Rev. Lett.* **98** 037401
[5] Mitrano M, Cotugno G, Clark S R, Singla R, Kaiser S, Stähler J, Beyer R, Dressel M, Baldassarre L, Nicoletti D, Perucchi A, Hasegawa T, Okamoto H, Jaksch D and Cavalleri A 2014 *Phys. Rev. Lett.* **112** 117801
[6] Chen W, Zhong H, Bao C, Wang F, Cai X, Yun C, Teng H, Wei Z and Zhou S 2025 *Chin. Phys. Lett.* **42** 017101
[7] Fausti D, Tobey R I, Dean N, Kaiser S, Dienst A, Hoffmann M C, Pyon S, Takayama T, Takagi H and Cavalleri A 2011 *Science* **331** 189
[8] Nicoletti D, Casandruc E, Laplace Y, Khanna V, Hunt C R, Kaiser S, Dhesi S S, Gu G D, Hill J P and Cavalleri A 2014 *Phys. Rev. B* **90** 100503
[9] Hu W, Kaiser S, Nicoletti D, Hunt C R, Gierz I, Hoffmann M C, Le Tacon M, Loew T, Keimer B and Cavalleri A 2014 *Nat. Mater.* **13** 705
[10] Kaiser S, Hunt C R, Nicoletti D, Hu W, Gierz I, Liu H Y, Le Tacon M, Loew T, Haug D, Keimer B and Cavalleri A 2014 *Phys. Rev. B* **89** 184516
[11] Yin X, Zhang J, Dong W, Nakagawa T, Xia C, Zhang C, Guo W, Chang J and Ding Y 2023 *Chin. Phys. B* **33** 016103
[12] Zhu J, Li Y X, Feng D M, Su D P, Fan D N, Yang S, Zhao C X, Zhao G Y, Li L, Li F F, Wang Y H and Zhou Q 2023 *Chin. Phys. B* **32** 067801
[13] Oka T, Arita R and Aoki H 2003 *Phys. Rev. Lett.* **91** 066406
[14] Oka T and Aoki H 2005 *Phys. Rev. Lett.* **95** 137601
[15] Maeshima N and Yonemitsu K 2005 *J. Phys. Soc. Jpn.* **74** 2671
[16] Takahashi A, Itoh H and Aihara M 2008 *Phys. Rev. B* **77** 205105
[17] Eckstein M, Oka T and Werner P 2010 *Phys. Rev. Lett.* **105** 146404
[18] Eckstein M and Werner P 2013 *Phys. Rev. Lett.* **110** 126401
[19] Shao C, Tohyama T, Luo H G and Lu H 2016 *Phys. Rev. B* **93** 195144
[20] Shinjo K and Tohyama T 2017 *Phys. Rev. B* **96** 195141
[21] Werner P, Li J, Golež D and Eckstein M 2019 *Phys. Rev. B* **100** 155130
[22] Rincón J and Feiguin A E 2021 *Phys. Rev. B* **104** 085122
[23] Werner P, Strand H U R, Hoshino S, Murakami Y and Eckstein M 2018 *Phys. Rev. B* **97** 165119
[24] Wang Y, Chen C C, Moritz B and Devereaux T P 2018 *Phys. Rev. Lett.* **120** 246402
[25] Bittner N, Tohyama T, Kaiser S and Manske D 2019 *J. Phys. Soc. Jpn.* **88** 044704
[26] Kaneko T, Shirakawa T, Sorella S and Yunoki S 2019 *Phys. Rev. Lett.* **122** 077002
[27] Wang Y, Shi T and Chen C C 2021 *Phys. Rev. X* **11** 041028
[28] Zhang Y, Mondaini R and Scalettar R T 2023 *Phys. Rev. B* **107** 064309
[29] Chen J, Petocchi F, Christiansson V and Werner P 2024 *Phys. Rev. B* **109** L201101
[30] Chollet M, Guerin L, Uchida N, Fukaya S, Shimoda H, Ishikawa T, Matsuda K, Hasegawa T, Ota A, Yamochi H, Saito G, Tazaki R, Adachi S and Koshihara S 2005 *Science* **307** 86
[31] Onda K, Ogihara S, Yonemitsu K, Maeshima N, Ishikawa T, Okimoto Y, Shao X, Nakano Y, Yamochi H, Saito G and Koshihara S 2008 *Phys. Rev. Lett.* **101** 067403
[32] Yonemitsu K and Maeshima N 2007 *Phys. Rev. B* **76** 075105
[33] Yonemitsu K, Maeshima N, Tanaka Y and Miyashita S 2009 *J. Phys. Conf. Ser.* **148** 012054
[34] Lee J D 2009 *Phys. Rev. B* **80** 165101
[35] Pedron D, Bozio R, Meneghetti M and Pecile C 1994 *Phys. Rev. B* **49** 10893
[36] Nishimoto S, Takahashi M and Ohta Y 2000 *J. Phys. Soc. Jpn.* **69** 1594
[37] Shibata Y, Nishimoto S and Ohta Y 2001 *Phys. Rev. B* **64** 235107
[38] Tsuchiizu M, Yoshioka H and Suzumura Y 2001 *J. Phys. Soc. Jpn.* **70** 1460
[39] Penc K and Mila F 1994 *Phys. Rev. B* **50** 11429
[40] Mila F 1995 *Phys. Rev. B* **52** 4788
[41] Favand J and Mila F 1996 *Phys. Rev. B* **54** 10425
[42] Benthien H and Jeckelmann E 2005 *Eur. Phys. J. B* **44** 287
[43] Le N H, Fisher A J, Curson N J and Ginossar E 2020 *npj Quantum Inf.* **6** 24
[44] Shao C, Tohyama T and Lu H 2024 *Phys. Rev. B* **110** 245121
[45] Jeckelmann E 2003 *Phys. Rev. B* **67** 075106
[46] Prelovšek P and Bonča J *Strongly Correlated Systems–Numerical Methods*, edited by A. Avella and F. Mancini, *Springer Series in Solid-State Sciences*, Vol. 176 (Berlin : Springer)
[47] Lenarčič Z, Golež D, Bonča J and Prelovšek P 2014 *Phys. Rev. B* **89** 125123
[48] Xu R H, Lu H, Tohyama T and Shao C 2025 *Phys. Rev. B* **112** 085131
[49] Lu H, Shao C, Bonča J, Manske D and Tohyama T 2015 *Phys. Rev. B* **91** 245117
[50] Shao C, Lu H, Luo H G and Mondaini R 2019 *Phys. Rev. B* **100** 041114